Inhomogeneous strain relaxation in etched quantum dots and wires: From strain distributions to piezoelectric fields and band-edge profiles

Y. M. Niquet
CEA-CNRS Joint Group ''Microstructures de Semiconducteurs II-VI,'' Laboratoire de Spectrométrie Physique, Université J. Fourier-Grenoble I, Boîte Postale 87, 38402 Saint Martin d'Hères, France and Institut d'Electronique et de Microélectronique du Nord, Departement ISEN, Boîte Postale 69, F-59652 Villeneuve d'Ascq Cedex, France

C. Priester
Institut d'Electronique et de Microélectronique du Nord, Département ISEN, Boîte Postale 69, F-59652 Villeneuve d'Ascq Cedex, France

C. Gourgon* and H. Mariette
CEA-CNRS Joint Group ''Microstructures de Semiconducteurs II-VI,'' Laboratoire de Spectrométrie Physique, Université J. Fourier-Grenoble I, Boîte Postale 87, 38402 Saint Martin d'Hères, France
(Received 6 November 1997)

Inhomogeneous strain relaxation in quantum dots etched from biaxially strained quantum wells is calculated. Strain-induced band effects and piezoelectric potentials are discussed for several wires and dots (mainly II-VI systems, but results are generalized to other zinc-blende systems such as $In_xGa_{1-x}As/GaAs$). General trends for varying design parameters of the nanostructures are given. Results are compared to data obtained from optical spectroscopy experiments. The case of a system under tensile strain that evidences an unexpected relaxation phenomenon is also discussed both experimentally and theoretically. [S0163-1829(98)02023-2]

I. INTRODUCTION

Quantum wires (QWR's) and quantum dots (QD's) etched from [001]-oriented quantum wells (QW's) have attracted much attention as a way to achieve one-dimensional (1D) and 0D nanostructures with a wide range of possible applications. Lateral confinement effects by air or vacuum have been reported for the smallest QWR's and QD's.[1–3] Moreover, strain relaxation is expected to play an important role in nanostructures etched from QW's, which are under biaxial strain due to the lattice mismatch with the underlying buffer layer. These QWR's and QD's indeed undergo a partial elastic relaxation in the vicinity of the sidewalls created by the patterning process. This can affect the properties of the whole structure depending on its lateral size as compared to the thickness of the strained QW. The consequences of strain relaxation on the electronic band structure can be large, even in QWR's and QD's that are much too large to expect 1D and 0D confinement effects. Optical results—such as energy shifts of the optical transition—have been qualitatively related to such relaxation effects.[4–6]

Simple models assuming a homogeneous strain relaxation in QWR'S and QD's have been used[7–9] to account *a posteriori* for experimental data, without taking into account the detailed distribution of strains in these structures. More detailed strain calculations are usually performed within continuous elasticity's framework, either using numerical methods such as finite elements, or more analytical methods such as Fourier series,[10] or Green's-functions methods. From the opposite point of view are performed atomistic calculations based on the valence force field model.[11] It should be noted that the accuracy of the valence force field model goes beyond classical elasticity theory and should also give a reasonable description of relaxation on an atomic scale.

Complete strain calculations, using finite elements[12,13] (FE), Fourier series (FS),[14,15] or Green's-functions methods[16,17] have been developed for related problems such as uniform stripes or semi-infinite media. More recently, calculations based on FS methods or Keating's valence force field (VFF) framework have been reported for the case of etched QWR's,[18–21] including the calculation of piezoelectric potentials and/or strain-induced band effects.

In this paper, we report some results for QWR's and a complete calculation of strain relaxation, strain-induced band effects, and piezoelectric potential in QD's, using FE and VFF methods. We compare these calculations with experimental data obtained from $CdTe/Cd_{0.85}Zn_{0.15}Te$ QWR's and QD's and from a system under tensile strains, $ZnTe/Zn_{0.80}Mg_{0.20}Te$.

In the next section we briefly present the VFF and FE methods and discuss typical strain fields in QD's. In Sec. III we calculate piezoelectric fields in QD's. Strain-induced band effects are given in Sec. IV. Finally, we compare in Sec. V the calculation with experimental data from $CdTe/Cd_{0.85}Zn_{0.15}Te$ and $ZnTe/Zn_{0.80}Mg_{0.20}Te$ QWR's and QD's.

II. STRAIN FIELDS IN QUANTUM DOTS

Strain fields in relaxed QWR's and QD's are calculated using either continuum elasticity theory (FE method) or Keating's VFF framework.

The VFF approximation models the elastic properties on the atomic scale.[22] The strain elastic energy δE depends on

the geometric deformations of bonds that each atom makes with his four nearest neighbors. For each atom i of the zinc-blende structure one can write:

$$\delta E_i = \sum_{j=1}^{4} \frac{3}{8 r_0^{\,2}} \alpha [\vec{r_{ij}}^{\,2} - r_0^{\,2}]^2 + \sum_{j=1}^{4} \sum_{k=j+1}^{4} \frac{3}{8 r_0^{\,2}} \beta \left[\vec{r_{ij}} \cdot \vec{r_{ik}} + \frac{r_0^{\,2}}{3} \right]^2 . \quad (1)$$

$\vec{r_{ij}}$ is the vector connecting the central atom i to one of its four nearest neighbors j; r_0 is the unstrained bond length; α and β are, respectively, bond-bending and bond-stretching elastic constants. They are related to the elastic constants c_{11}, c_{12}, and c_{44} of the continuum elasticity theory by the following expressions:

$$c_{11} = \frac{\alpha + 3\beta}{a}; \quad c_{12} = \frac{\alpha - \beta}{a}; \quad c_{44} = \frac{4\alpha\beta}{a(\alpha+\beta)}. \quad (2)$$

$a = 4r_0/\sqrt{3}$ is the lattice constant. It is not possible to perfectly fit all three c_{ij}'s with only two elastic constants α and β; the less ionic the material, the better the fit. Thus, this method basically works with covalent bonding, but Coulomb corrections could be introduced.[23] In practice, for the sake of simplicity one usually simply uses Eq. (1).[24] We do this, and choose to fit c_{11} and c_{12} and to drop c_{44}, resulting in a 10–20 % error range on the VFF effective c_{44}. We do not account for surface reconstruction. This is justified for structures with high enough volume to surfaces ratios. VFF calculations allow us to search for the effect of anistropy in small structures and for the effects of the specific distribution of atoms on the relaxation especially near free surfaces.

FE methods are very general and apply to any geometry. The elastic medium is assumed to be isotropic and the strain elastic energy density is given in the $\{\vec{x}' = [100], \vec{y}' = [010], \vec{z}' = [001]\}$ axis set by

$$\delta U = \tfrac{1}{2} c_{11} (\epsilon_{x'x'}^2 + \epsilon_{y'y'}^2 + \epsilon_{z'z'}^2) + c_{12} (\epsilon_{x'x'}\epsilon_{y'y'} + \epsilon_{x'x'}\epsilon_{z'z'} + \epsilon_{y'y'}\epsilon_{z'z'}) + 2c_{44} (\epsilon_{x'y'}^2 + \epsilon_{z'x'}^2 + \epsilon_{z'y'}^2). \quad (3)$$

However, small features such as monoatomic steps cannot be reproduced as accurately as in VFF framework.

In both VFF and FE methods, we search for the strain fields in relaxed QWR's and QD's by minimizing the total elastic energy with respect to the ϵ_{ij} or to the atomic positions when the structure is allowed to relax an initial biaxial strain.

We have performed these calculations for various QWR's and square-shaped QD's etched from single [001] (z axis) strained QW's. A typical QD geometry is shown in Fig. 1. The wire and dot widths are labeled L_{QWR} and L_{QD}, respectively. The well thickness is labeled L_{QW}. The wires are oriented along the $\vec{y} = [110]/\sqrt{2}$ direction and the dots along the $\vec{x} = [1\bar{1}0]/\sqrt{2}$ and $\vec{y} = [110]/\sqrt{2}$ directions. After etching, wires can relax strains by the two $[1\bar{1}0]$ lateral edges on

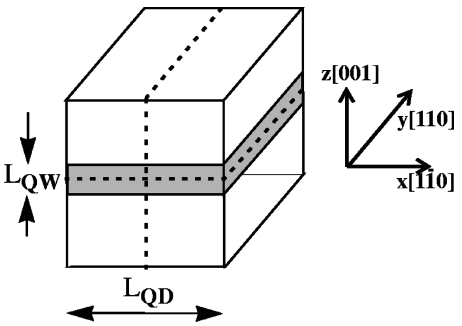

FIG. 1. Typical QWR and QD geometries. The QWR's are oriented along the [110] direction and the QD's are oriented along the [110] and $[1\bar{1}0]$ directions. A ''horizontal'' $(\vec{x},\vec{y})$ plane and the middle vertical $(\vec{x},\vec{z})$ plane are shown as dotted lines.

which stresses vanish. Therefore, only ϵ_{yy} remains imposed by the buffer, the shear strains ϵ_{xy} and ϵ_{zy} being zero in the whole structure. On the opposite, QD's can relax in-plane strains in both x ($[1\bar{1}0]$) and y ([110]) directions.

We have especially investigated the case of one III-V and two II-VI QWR's and QD's for which numerous experimental data are available, namely, (i) $Ga_{0.82}In_{0.18}As$(QW)/GaAs (barriers and buffer)[25,26] with lattice mismatch:

$$\epsilon_{\parallel} = \frac{a_{\mathrm{GaAs}} - a_{\mathrm{Ga_xIn_{1-x}As}}}{a_{\mathrm{Ga_xIn_{1-x}As}}} = -1.27\%, \quad (4)$$

(ii) $Zn_{0.80}Cd_{0.20}Se/ZnSe$[1,5,6,27] (blue laser system), with $\epsilon_{\parallel} = -1.43\%$, (iii) $CdTe/Cd_{0.85}Zn_{0.15}Te$,[8] with $\epsilon_{\parallel} = -0.88\%$.

As a case of tensile strain, $ZnTe/Zn_{0.80}Mg_{0.20}Te$ systems have also been considered and experimentally investigated ($\epsilon_{\parallel} = +1.03\%$). All lattice parameters and elastic constants are taken from Ref. 28 for binary compounds, except for the lattice parameter of cubic MgTe, taken from Ref. 29. They are extrapolated to ternary alloys using Vegard's law. However, in the absence of reliable elastic constants for cubic CdSe and MgTe, the values used for $Zn_{0.80}Cd_{0.20}Se$ and $Zn_{0.80}Mg_{0.20}Te$ are those of ZnSe and ZnTe, respectively.

Typical results for QWR's have been reported in earlier papers[18,19] and the reader is referred to these papers for a detailed discussion about strain fields in relaxed QWR's. FE results for a 80-nm-wide $CdTe/Cd_{0.85}Zn_{0.15}Te$ QD ($L_{\mathrm{QW}} = 100$ Å) are shown in Figs. 2 and 3. The strain fields ϵ_{yy}, ϵ_{zz}, and ϵ_{xy} are plotted in a ''horizontal'' $(\vec{x},\vec{y})$ plane in the center of the CdTe QW. The shear strain ϵ_{zx} is plotted at the upper interface of the QW where it reaches its maximum value. The strain deformation ϵ_{yy} rapidly decreases along the y axis close to the [110] free edges where it exhibits a singularity characteristic of heterojunction-gas interfaces.[30] On the opposite, ϵ_{yy} does not show strong variations along the x axis close to the $[1\bar{1}0]$ free edges, since the motion of atoms along the y axis is weakly influenced by the existence of stress-free surfaces in the x direction. The strain deformation ϵ_{xx} (not represented here) can be deduced from ϵ_{yy} by a simple permutation of x and y axes. The strains ϵ_{xx} and ϵ_{yy} are partly relaxed in the center of the structure, that is, $\epsilon_{xx} = \epsilon_{yy} = 0.77\epsilon_{\parallel}$. The strain component ϵ_{zz} is the only one that has the full fourth-order symmetry of the QD. It also exhibits solid-gas interface singularities at the free edges and corners.

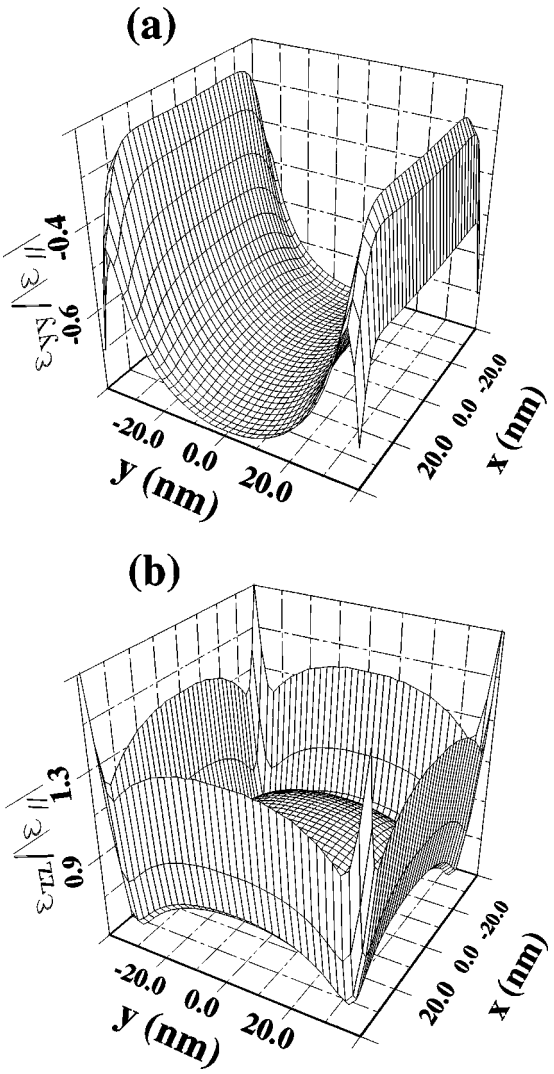

FIG. 2. Strain deformations ϵ_{xx} (a) and ϵ_{zz} (b) plotted in a horizontal $(\vec{x},\vec{y})$ plane in the center of the CdTe QW of a $CdTe/Cd_{0.85}Zn_{0.15}Te$ QD ($L_{QD}=80$ nm, $L_{QW}=100$ Å, $\epsilon_{\parallel}=-0.66\%$) (FE calculation).

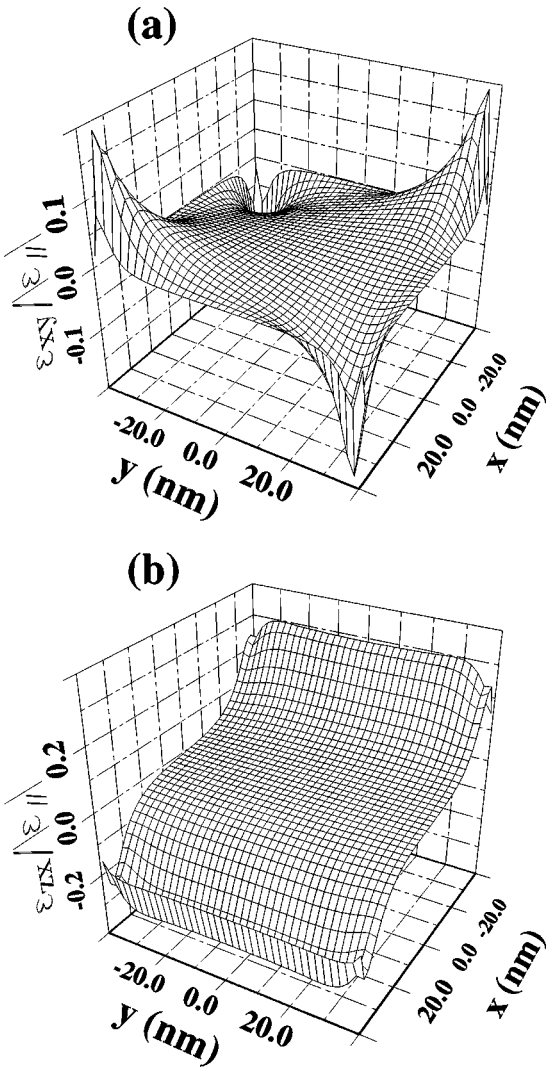

FIG. 3. (a) Shear strain ϵ_{xy} plotted in the center of the CdTe QW of the same $CdTe/Cd_{0.85}Zn_{0.15}Te$ QD as in Fig. 2. (b) Shear strain ϵ_{zx} plotted at the upper interface of the CdTe QW where it reaches its maximum (FE calculation).

The corners of the QD are the most distorted parts of the structure and show strong in-plane shear strain ϵ_{xy}. The shear strain ϵ_{zx} is maximum at the heterointerfaces and, like ϵ_{xx}, is weakly sensitive to the y coordinate. The shear strain ϵ_{zy} can be deduced from ϵ_{zx} by a permutation of x and y axes.

A vertical section in the middle $(\vec{x},\vec{z})$ plane of this QD ($y=0$) exhibits roughly the same features as a vertical section of the corresponding QWR ($L_{QWR}=80$ nm, $L_{QW}=100$ Å).[18,19] The strains ϵ_{xx}, ϵ_{yy}, ϵ_{zz} show small variations with the z coordinate in the QW but the shear strains ϵ_{zx} and ϵ_{zy} change their sign from the lower to the upper interface. The shear strain ϵ_{xy} is maximum in the center of the QW. The barriers are distorted by the relaxation in the QW. Due to lattice commensurability, the in-plane strains ϵ_{xx} and ϵ_{yy} in the barriers are proportional, close to the interfaces, to the strain relief in the QW. They rapidly decrease far from the interfaces.

Similar results can be obtained for small QD's within a VFF framework. However, QD's calculated with VFF model are a bit more relaxed and exhibit stronger shear strains ϵ_{zx} and ϵ_{zy} than QD's calculated with FE methods. As an example, in a 20-nm-wide $Zn_{0.80}Cd_{0.20}Se/ZnSe$ QD ($L_{QW}=25$ Å), we get in the center of the structure $\epsilon_{xx}=\epsilon_{yy}=0.740\epsilon_{\parallel}$ with VFF calculations and $\epsilon_{xx}=\epsilon_{yy}=0.755\epsilon_{\parallel}$ with FE methods. The maximum shear strains at the heterointerfaces are, respectively, $\epsilon_{zx}=\epsilon_{zy}=0.388|\epsilon_{\parallel}|$ (VFF) and $\epsilon_{zx}=\epsilon_{zy}=0.336|\epsilon_{\parallel}|$ (FE). This is due to a weak effective c_{44} within VFF framework. Moreover, the solid-gas interface singularity at the edges is attenuated with VFF methods due to the discrete structure of the atomic distribution.

In order to compare different structures, we have defined a relaxation ratio ρ and an aspect ratio χ for QWR's and QD's:

$$\chi=\frac{L_{QWR}}{L_{QW}}(\text{wires}) \quad \text{and} \quad \chi=\frac{L_{QD}}{L_{QW}}(\text{dots}), \tag{5}$$

$$\rho=1-\frac{\epsilon_{xx}^{0}}{\epsilon_{\parallel}}. \tag{6}$$

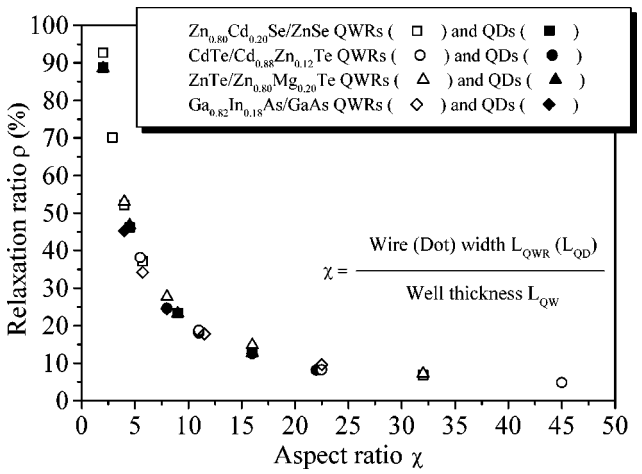

FIG. 4. Relaxation ratio ρ vs aspect ratio χ for different III-V or II-VI QWR's and QD's. This curve can be viewed as a universal one, which applies to many other structures (VFF calculation).

$\epsilon^0_{\alpha\beta}$ is the calculated strain at the center of the relaxed QWR or QD (in this latter case, $\epsilon^0_{xx}=\epsilon^0_{yy}$). The higher is the relaxation ratio, the more relaxed is the structure. Let us emphasize that ρ is not sufficient to fully determine the strain state at the center of the QWR or QD: every shear strain vanishes, but the vertical strain ϵ^0_{zz} cannot be deduced from the in-plane strains ϵ^0_{xx} and ϵ^0_{yy} with the usual ''biaxial'' law:

$$\epsilon^0_{zz}=-\frac{c_{12}}{c_{11}}(\epsilon^0_{xx}+\epsilon^0_{yy}), \tag{7}$$

as the vertical stress σ_{zz} is nonzero due to lattice plane bending. As an example, for an 80-nm-wide CdTe (ZnSe) QD ($L_{\mathrm{QW}}=100$ Å), ϵ^0_{zz} is only 90% (86%) of the value given by Eq. (7). We have shown[19,20] ρ to depend only on χ, as soon as the etched buffer and cap layer are thick enough to prevent these whole layers from being highly strained. The evolution of the relaxation ratio with the aspect ratio for both QWR's and QD's is shown in Fig. 4. As expected, it decreases with increasing χ, that is, with increasing the wire or dot width, or decreasing the well thickness. Strain relaxation in QWR's and QD's originates at the surfaces. It is very effective close to the edges over a distance two to three times L_{QW}, but is weaker deep inside the structures. The QWR's and QD's with smallest χ exhibit very high relaxation ratios. We have found that the stress could even turn to an overrelaxation ($\rho>1$) in the center of the QWR's (QD's) when $\chi<1.5$. In such cases, ρ is no longer a good parameter for describing the relaxation, since the distribution of strains is far too inhomogeneous and exhibits strong gradients, both along the wire (dot) width and along the growth axis. The QWR's and QD's data are distributed along the same curve, but QD's relax in-plane strain in both x and y directions (that is, $\epsilon^0_{xx}=\epsilon^0_{yy}$), whereas QWR's relax in-plane strains only across the wire width (that is $\epsilon_{yy}=\epsilon_{\parallel}$). Hence, the strain elastic energy density in the center of a QD is far lower than in the corresponding QWR. Moreover, the relaxation ratio does not depend significantly on the nature of the materials constituting the structures, since elastic constants are usually of the same order in QW's and barriers. This curve $\rho(\chi)$ can therefore be seen as a universal one, which applies to both QWR's and QD's and to a lot of covalent, III-V or II-VI materials. The relaxation ratio ρ appears to decrease linearly with $1/(\chi-\chi_0)$ in the range $2\leqslant\chi\leqslant45$, with $\chi_0=0.52$.

III. PIEZOELECTRIC FIELDS

The strain fields induce a piezoelectric polarization field due to the relative displacement of the cations with respect to the anions in the lattice. The polarization density is given in the $\{\vec{x}=[1\bar{1}0]/\sqrt{2},\vec{y}=[110]/\sqrt{2},\vec{z}=[001]\}$ axis set by[31]

$$\begin{aligned} P_x&=-2e_{14}\epsilon_{zx},\\ P_y&=2e_{14}\epsilon_{zy},\\ P_z&=e_{14}(\epsilon_{yy}-\epsilon_{xx}). \end{aligned} \tag{8}$$

e_{14} is the piezoelectric constant [$e_{14}=0.049$ C/m^2 for ZnSe and $Zn_{0.80}Cd_{0.20}Se$ (Ref. 28)]. Note that, in [110] oriented QWR's, P_y is zero and P_x and P_z have translational invariance along the wire direction. This nonuniform piezoelectric polarization field gives rise to a piezoelectric potential given, in the absence of free electric charges, by

$$V_p(\vec{r})=\frac{1}{4\pi\epsilon_0\epsilon_r}\int\int\int\frac{\vec{P}(\vec{r}')(\vec{r}-\vec{r}')}{|\vec{r}-\vec{r}'|^3}d^3\vec{r}'. \tag{9}$$

ϵ_0 is the vacuum permittivity and ϵ_r is the relative dielectric constant, which is assumed to be constant in the whole structure [$\epsilon_r=8.7$ for ZnSe (Refs. 21 and 28)]. Due to translational invariance, this reduces, in QWR's, to:

$$V_p(\vec{r})=\frac{1}{2\pi\epsilon_0\epsilon_r}\int\int\frac{\vec{P}(\vec{r}')(\vec{r}-\vec{r}')}{|\vec{r}-\vec{r}'|^2}d^2\vec{r}'. \tag{10}$$

Another way to get piezoelectric potentials is to integrate the equivalent density of bound charges given by

$$\begin{aligned} \rho_p(\vec{r})&=-\vec{\nabla}\cdot\vec{P}\quad\text{(in the bulk)},\\ \sigma_p(\vec{r})&=\vec{P}\cdot\vec{n}\quad\text{(on the surfaces)}. \end{aligned} \tag{11}$$

The piezoelectric density of charges ρ_p in an 80-nm-wide $Zn_{0.80}Cd_{0.20}Se$/ZnSe QWR ($L_{\mathrm{QW}}=100$ Å) is shown in Fig. 5 and the piezoelectric potential V_p is shown in Fig. 6. Due to translational invariance along the y axis, these bound charges have a stringlike structure.[18] It exhibits rather complicated features at the intersections between the heterointerfaces and the sidewalls, where ϵ_{xx} and ϵ_{zx} rapidly vary but give opposite contributions to ρ_p. There is a residual density of piezoelectric charges deep inside the barriers where both ϵ_{xx} and ϵ_{zx} contributions, although small, become of the same sign. This residual density of charges is maximum at the heterointerfaces. It is responsible for the slow decay of the piezoelectric potential inside the wire. Hence the piezoelectric potential in this QWR can be as large as ±35 mV, but the maximum is located in the barriers. The maximum piezoelectric potential in the QW is ±11.5 mV, which corresponds to piezoelectric fields of order 23 kV/cm. For larger wires, the maximum is pushed farther inside the barriers, with a decrease of the piezoelectric fields. For thicker QW's,

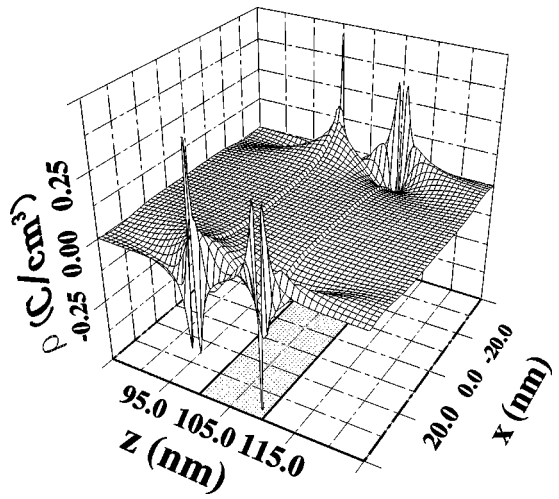

FIG. 5. Piezoelectric density of charges ρ_p in a $Zn_{0.80}Cd_{0.20}Se/ZnSe$ QWR ($L_{QWR}=80$ nm, $L_{QW}=100$ Å). The position of the $Zn_{0.80}Cd_{0.20}Se$ QW is shaded in the background (FE calculation).

the maximum piezoelectric potential in the QW increases, due to larger relaxation as well as higher spacing of the charges.

The piezoelectric potential V_p in an 80-nm-wide $Zn_{0.80}Cd_{0.20}Se/ZnSe$ QD ($L_{QW}=100$ Å) is shown in Fig. 7. V_p is plotted in a horizontal plane at the upper interface of the $Zn_{0.80}Cd_{0.20}Se$ QW in Fig. 7(a), and in the middle vertical plane in Fig. 7(b). The piezoelectric potential exhibits four extremas, corresponding to ± 7.5 mV, in the growth plane close to the sidewalls (note by comparing Figs. 6 and 7 that, for similar sizes, the maximum piezoelectric potentials are much lower in QD's than in QWR's). The $[110]$ and $[1\bar{1}0]$ sidewalls carry opposite charges, which is responsible for the particular symmetry of V_p. V_p always vanishes along the diagonals and the axis of symmetry of the QD, as long as it remains square shaped.

As the strain fields are mainly dependent on the aspect ratio χ, the piezoelectric potential in QWR's and QD's can be scaled with the dimensions of the structure. For example,

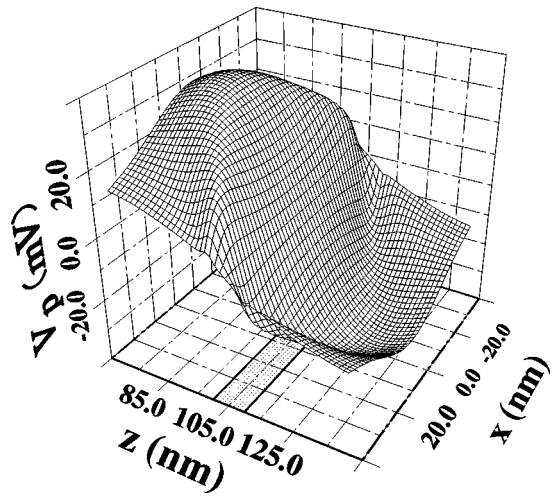

FIG. 6. Piezoelectric potential V_p in a $Zn_{0.80}Cd_{0.20}Se/ZnSe$ QWR ($L_{QWR}=80$ nm, $L_{QW}=100$ Å) (FE calculation).

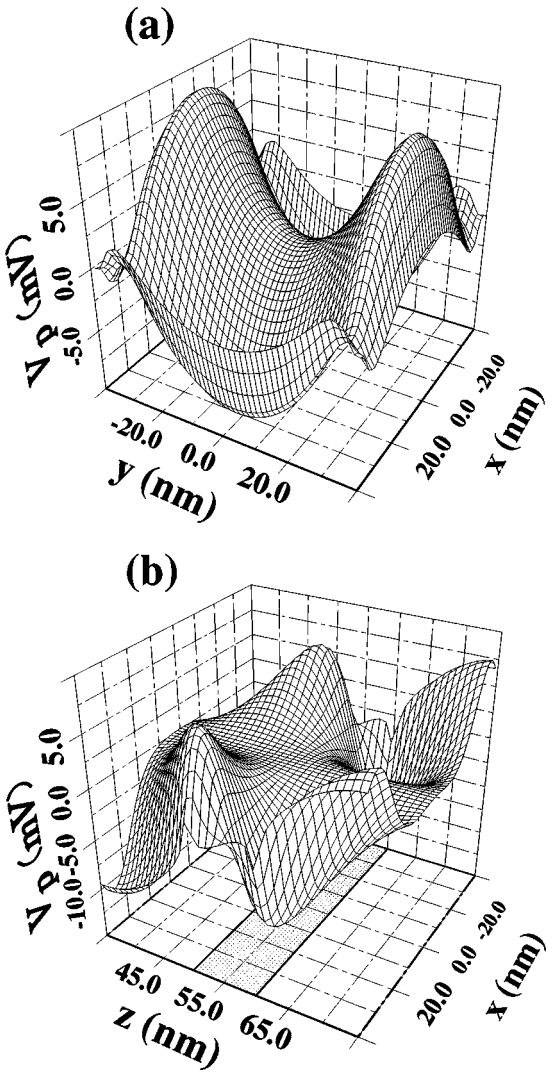

FIG. 7. Piezoelectric potential V_p in a $Zn_{0.80}Cd_{0.20}Se/ZnSe$ QD plotted at the upper interface (a) or in the middle vertical $(\vec{x},\vec{z})$ plane (b) ($L_{QD}=80$ nm, $L_{QW}=100$ Å). The position of the $ZnSeZn_{0.80}Cd_{0.20}Se$ QW is shaded in the background (FE calculation).

an 80-nm-wide QWR (QD) with a 100-Å-thick QW exhibits twice the piezoelectric potential of a 40-nm-wide QWR (QD) with a 50-Å-thick QW.

The effect of the piezoelectric potential on the optical properties of the nanostructures is to lower the energy of the optical transitions. If V_p is high enough compared to the confinement energies (typically for $L_{QW} \geqslant 100$ Å), the electrons and holes will be localized, respectively, in the maxima and minima of the piezoelectric potential.[32] This will downshift the optical transition. This effect is expected to be of less importance in QD's, due to the symmetry of the charge distribution: strong piezoelectric fields exist in the whole QWR, whereas the piezeolectric potential is weaker in QD's and vanishes in the center of the structure.

IV. STRAIN-INDUCED BAND-GAP ENERGY SHIFTS

Strain relaxation in QD's will induce changes in the bandgap energy and thus energy shifts of the optical transitions. We have calculated the strain induced bandgap energy shift

at $\vec{k}=0$, solving the Bir and Pikus strain Hamiltonian[33] in the $\{\vec{x}=[1\bar{1}0]/\sqrt{2},\vec{y}=[110]/\sqrt{2},\vec{z}=[001]\}$ axis set. For conduction and valence bands we get, respectively,

$$\Delta E_c = a_c \frac{\delta V}{V}, \tag{12}$$

$$\Delta E_v^{\pm} = a_v \frac{\delta V}{V} \pm \frac{1}{2}\sqrt{A+B}, \tag{13}$$

where

$$\frac{\delta V}{V} = \epsilon_{xx}+\epsilon_{yy}+\epsilon_{zz} \tag{14}$$

is the relative volume change, and

$$A = b^2[(2\epsilon_{zz}-\epsilon_{xx}-\epsilon_{yy})^2+12\epsilon_{xy}^2],$$

$$B = d^2[(\epsilon_{xx}-\epsilon_{yy})^2+4\epsilon_{zx}^2+4\epsilon_{zy}^2]. \tag{15}$$

a_c and a_v are the hydrostatic band-gap deformation potentials; the two other deformation potentials b and d describe the effect of tetragonal or trigonal distortions and shear deformations. For purely tetragonal distortion in compressive layers (e.g., biaxially strained layers), the ground state ΔE_v^+ corresponds to the ''heavy'' $|\frac{3}{2},\pm\frac{3}{2}\rangle$ hole and ΔE_v^- to the ''light' $|\frac{3}{2},\pm\frac{1}{2}\rangle$ hole. In other cases, the energy eigenstates ΔE_v^+ and ΔE_v^- are mixed states of the $|\frac{3}{2},\pm\frac{1}{2}\rangle$ and $|\frac{3}{2},\pm\frac{3}{2}\rangle$ holes but will still be referred to as heavy and light hole bands, respectively. All parameters are taken from Ref. 28 for ZnSe and $Zn_{0.80}Cd_{0.20}Se$.

The total confinement potential for electrons or holes is the sum of the unstrained band offsets, the strain-induced band-gap energy shift and the piezoelectric potential. The conduction-band (CB) and heavy-hole valence-band (VB) energies E_c and E_{hh} are shown in Figs. 8 and 9 for the same $Zn_{0.80}Cd_{0.20}Se/ZnSe$ QD as in the last section. E_c and E_{hh} are plotted in a horizontal plane in the center of the $Zn_{0.80}Cd_{0.20}Se$ QW in Figs. 8(a) and 9(a), and in the middle vertical plane in Figs. 8(b) and 9(b). The zero energies for the valence and conduction bands are, respectively, the unstrained VB and CB energies in the $Zn_{0.80}Cd_{0.20}Se$ QW. The piezoelectric potential is nearly zero in the center of the $Zn_{0.80}Cd_{0.20}Se$ QW so that the variations of E_c and E_{hh} in Figs. 8(a) and 9(a) are those of the Bir and Pikus strain Hamiltonian energies ΔE_c and ΔE_v^+.

The confinement potentials E_c and $-E_{hh}$ abruptly decrease close to the sidewalls due to strong relaxation (which means an increase in the relative volume change $\delta V/V$ towards positive values), and to strong shear strains. The depth of the ''triangular'' wells appearing at the edges with respect to the CB and VB extrema is up to 45 meV in the conduction band and 15 meV in the valence band. They are about 10 nm thick. This strong decrease of the CB and VB energies at the edges will help the diffusion of the free carriers from the center of the QD towards the edges where they may be confined in the triangular wells. In large structures, this would lead to optical transitions from the edges redshifted with respect to the ones from the center of the structure.[25] However, most carriers may be trapped on nonradiative etching defects.[34] This would decrease the radiative efficiency of small QD's. It is worth noticing that in systems under tensile strains, such as $ZnTe/Zn_{0.80}Mg_{0.20}Te$ QD's, a strong increase of the CB and VB energies is expected close to the edges, as already pointed out for QWR's.[19] This should prevent important carrier diffusion towards nonradiative etching defects.

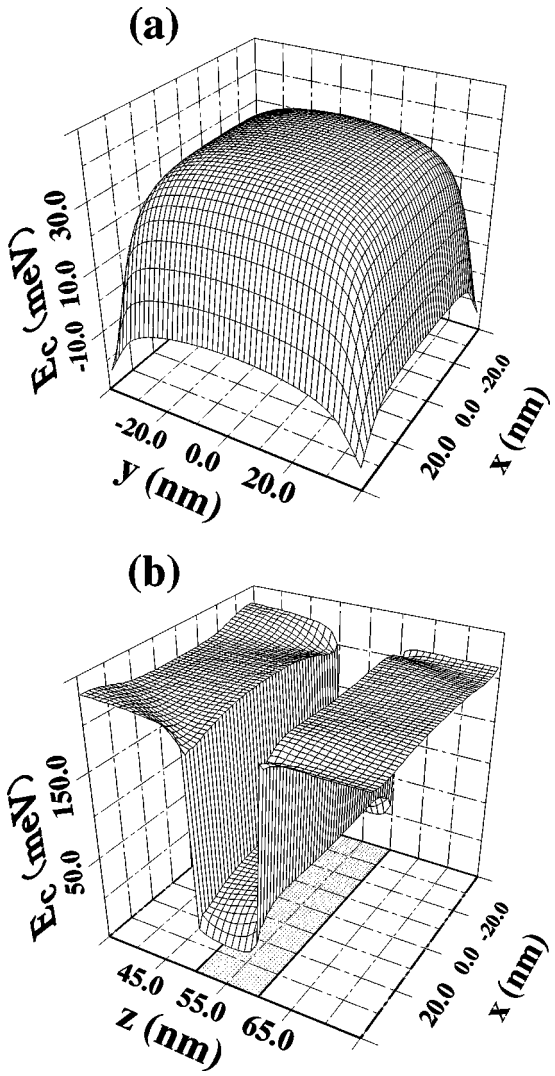

FIG. 8. Conduction-band energy E_c in a $Zn_{0.80}Cd_{0.20}Se/ZnSe$ QD plotted in the center of the $Zn_{0.80}Cd_{0.20}Se$ QW (a) or in the middle vertical plane (b) ($L_{QD}=80$ nm, $L_{QW}=100$ Å) (FE calculation).

The variation $\Delta E_g = E_c - E_{hh}$ of the band-gap energy with respect to the unstrained band gap is $\Delta E_g = 27.3$ meV in the center of the QD structure and $\Delta E_g = 21.4$ meV in the unetched 2D QW. Thus, the shift of the band-gap energy in the center of the QD structure with respect to the 2D QW is $\Delta E_{QD} = 5.9$ meV. The band-gap energy does not decrease towards the unstrained band gap in the center of the QD structure because the strain state is not representative of the biaxial case (see Sec. II). An 8-meV redshift is experimentally observed in 80-nm-wide $Zn_{0.80}Cd_{0.20}Se/ZnSe$ QD's.[6] It has, however, been shown that the strong decrease of CB and VB energies close to the edges should be taken into account in $Zn_{0.80}Cd_{0.20}Se/ZnSe$ QWR's and QD's for describing more accurately experimental data.[20,21]

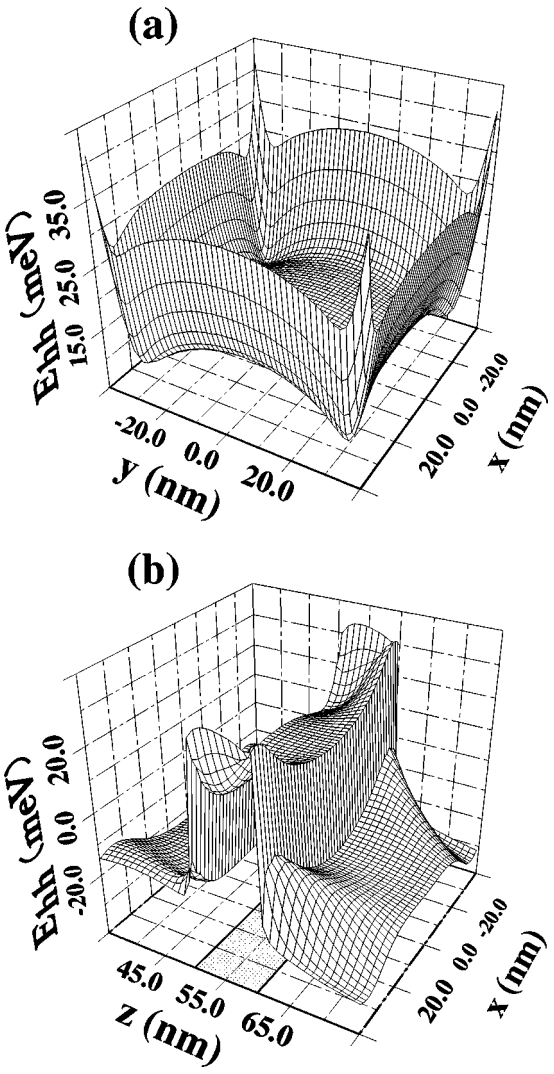

FIG. 9. Valence-band (heavy hole) energy E_{hh} plotted in the center of the $Zn_{0.80}Cd_{0.20}Se$ QW (a) or in the middle vertical plane (b) ($L_{\mathrm{QD}}=80$ nm, $L_{\mathrm{QW}}=100$ Å) (FE calculation).

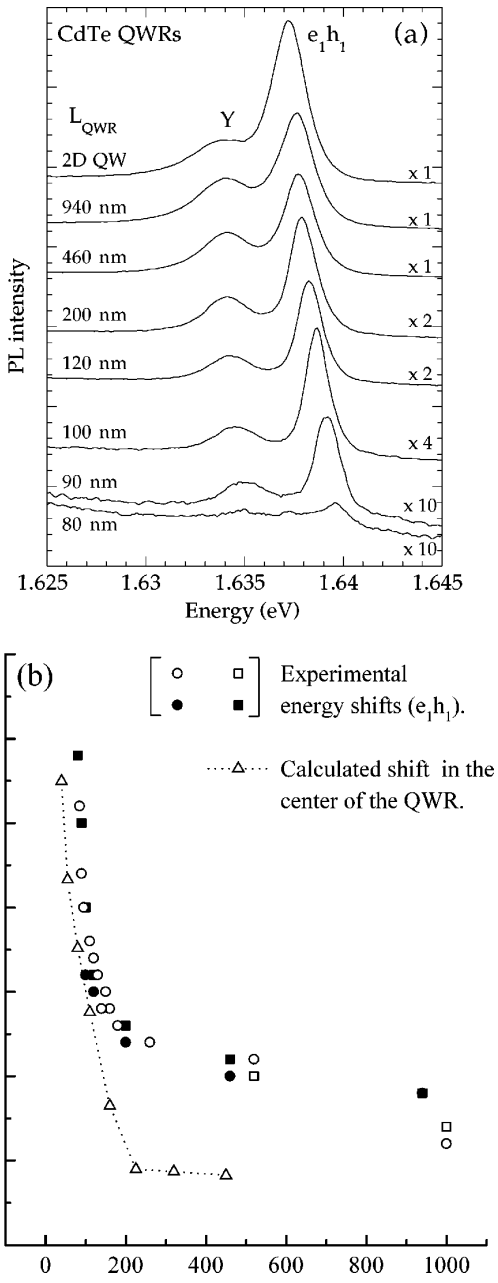

FIG. 10. (a) PL spectra for $CdTe/Cd_{0.85}Zn_{0.15}Te$ QWR's with 50-Å-thick QW's and various lateral sizes. (b) The e_1h_1 blueshifts with respect to the strained QW are reported together with calculated band-gap energy shifts in the center of the structures. For the significance of open (closed) squares and circles, see text Sec. V (VFF calculation).

V. COMPARISON WITH EXPERIMENTAL DATA

Experimental photoluminescence (PL) spectra for $CdTe/Cd_{0.85}Zn_{0.15}Te$ QWR's with various lateral sizes are shown in Fig. 10(a).[8] The shifts of the e_1h_1 excitonic peak with respect to the unetched strained QW are reported in Fig. 10(b) for QWR's and in Fig. 11 for QD's. The QW's are 50 Å thick ($\epsilon_{\parallel}=-0.88\%$). The samples were etched in an ion beam etching (IBE) machine under Ar^+ flux. A first set of PL spectra (open symbols) was taken at 2 K under either resonant (squares) or nonresonant (circles) excitations using an Ar laser. An anodic oxydation-deoxydation was then performed for additional etching and cleaning of the surface from the damaged layer created by the etching process.[35,36] A second set of PL spectra (solid symbols) was finally taken in the same conditions.

The calculated band-gap energy shifts in the center of the QWR's or QD's are also reported in Figs. 10(b) and 11. The piezoelectric fields have little influence since the QW is rather thin, which means low piezoelectric potentials (at most ± 0.9 mV at the edges in 80-nm-wide QWR's) as well as high confinement energies. Moreover, the decrease of CB and VB energies close to the sidewalls is far lower than in the former ZnSe structures (10 meV in each band in 80-nm-wide QWR's) and occurs very close to the edges (about 5 nm). As a consequence, the CB and VB energies in $CdTe/Cd_{0.85}Zn_{0.15}Te$ QWR's and QD's look rather flat as compared to the ZnSe structures. For calculating energy shifts, we ignore lateral confinement effects, which is valid as long as the wire/dot size does not fall below twice the 2D exciton radius ($\ll 250$ Å). Although the band-gap energy in the center of the QWR or QD cannot supersede a complete diagonalization of the Hamiltonian of the system, it can give some basic results about the influence of strain relaxation on

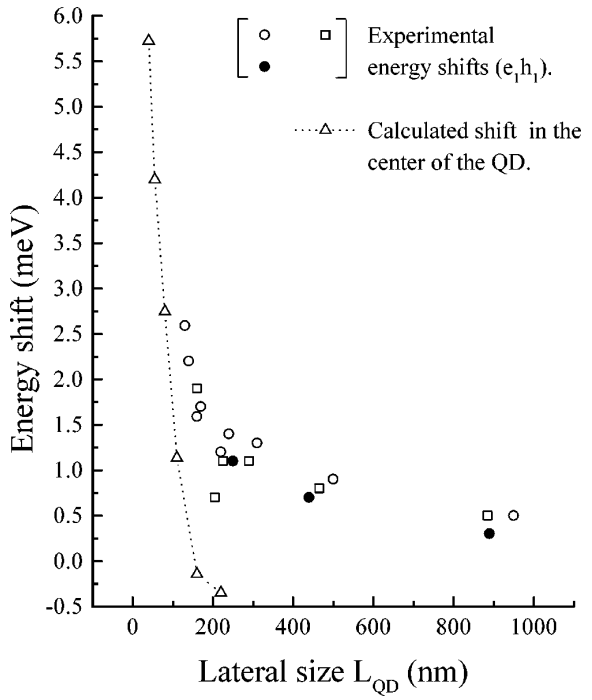

FIG. 11. The e_1h_1 blueshifts for $CdTe/Cd_{0.85}Zn_{0.15}Te$ QD's with 50-Å-thick QW's and various lateral sizes are reported together with the calculated band-gap energy shifts in the center of the structures. For the significance of open (closed) squares and circles, see text Sec. V (FE calculation).

the photoluminescence of the nanostructures. The calculated blueshifts in QWR's are about 0.5 meV lower than the experimental values, especially in wide wires, but the kink in the curve takes place at about 200 nm for both experimental and calculated data. Therefore strain relaxation is expected to have significant effects on the PL of these CdTe QWR's for lateral widths below 200 nm. The difference between calculated and experimental energy shifts could be attributed to some Zn/Cd interdiffusion during the ecthing process.[35] The calculated blueshifts in QD's can be very large (up to 5.75 meV in 40-nm-wide QD's), but decrease more rapidly than experimental values. Strain relaxation seems to have significant effects on the band edges energies of CdTe QD's for lateral widths below 160 nm. A complete calculation, taking into account the detailed variations of the CB and VB energies and effective masses, is now necessary to have a better interpretation of the experimental data but is beyond the scope of this paper.

The $ZnTe/Zn_{0.80}Mg_{0.20}Te$ system is a new system under tensile strains ($\epsilon_{\parallel} = +1.03\%$). The ground state in the ZnTe QW's is the e_1l_1 light exciton. In tensile layers, both the hydrostatic and shear terms of Eqs. (12) and (13) tend to lower the gap, whereas in compressive layers, these terms are of opposite signs and tend to cancel each other. This is why band gaps are usually much more sensitive to tensile strains than to compressive strains. The band-gap energy is decreased as much as 77 meV in the biaxially strained ZnTe QW's. According to our model, the optical transitions in the smallest $ZnTe/Zn_{0.80}Mg_{0.20}Te$ QWR's and QD's should be blueshifted some 10 meV with respect to the unetched strained QW. Moreover, the band-gap energy increases a lot close to the sidewalls, which should limit the diffusion of

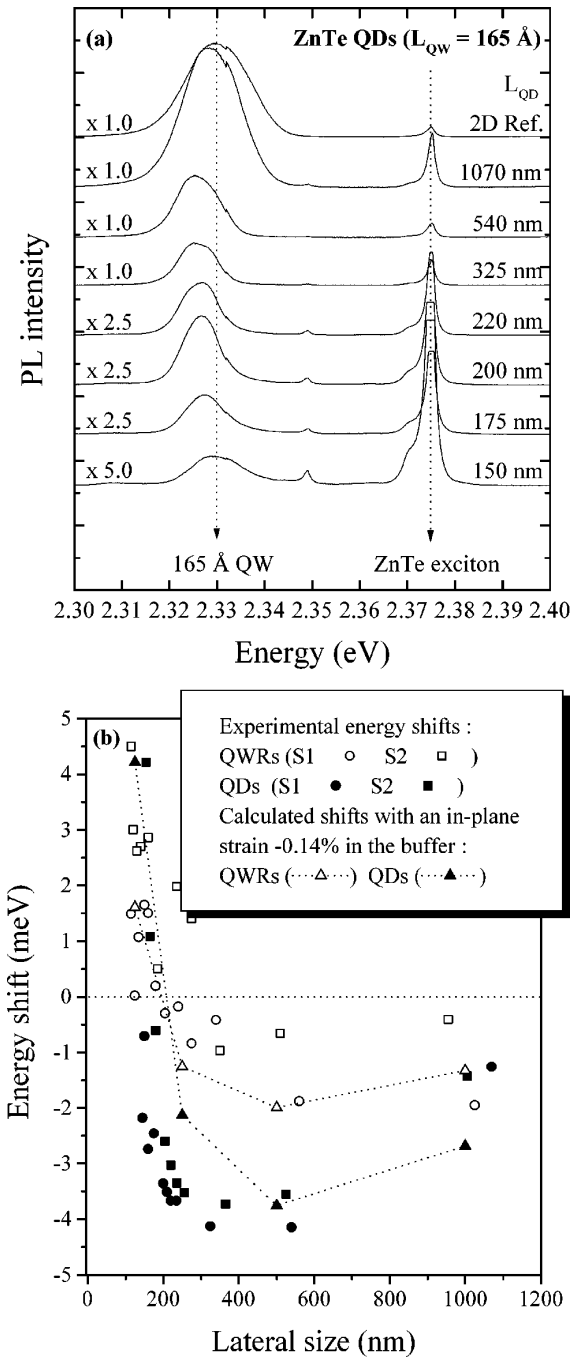

FIG. 12. (a) PL spectra for $ZnTe/Zn_{0.80}Mg_{0.20}Te$ QD's with 165-Å and 25-Å-thick QW's and various lateral sizes. (b) The e_1l_1 shifts in the 165-Å-thick QW are reported for wires and dots. The heterostructure was cleaved after growth into two samples S1 and S2. The calculated band-gap energy shifts in the center of the structures when a remaining in-plane strain $\epsilon = -0.14\%$ is imposed at the top of the buffer are also shown (FE calculation).

free carriers towards the edges, as pointed out in the last section.

The samples were grown by molecular beam epitaxy on [001]-oriented ZnTe substrates at 320 °C under excess of zinc (Zn:Te=2:1). Two ZnTe QW's are strained by a 2-μm-thick $Zn_{0.80}Mg_{0.20}Te$ buffer layer (lattice mismatch $\epsilon_{\parallel} = +1.03\%$). They are, respectively, 25 and 165 Å thick, and are separated by a 500-Å-thick $Zn_{0.80}Mg_{0.20}Te$ barrier. The whole heterostructure is capped with a 1000-Å-thick

$Zn_{0.80}Mg_{0.20}Te$ layer. The samples were etched in a IBE machine under Ar^+ flux. PL experiments were done at 2 K with an Ar laser (nonresonant excitations) operating in the near UV range. Typical PL spectra for QD's with various lateral sizes shown in Fig. 12(a). The energy shifts of the e_1l_1 transitions of the 165-Å-thick QW with respect to the unetched strained QW are reported in Fig. 12(b) for both QWR's and QD's.

The overall energy variation of the excitonic transition as a function of lateral size ($\Delta e_1l_1=9$ meV) is much larger than the one observed for CdTe nanostructures ($\Delta e_1h_1=2.5$ meV) as expected. However, the 165-Å-thick QWR's and QD's exhibit strong redshift even in large structures where no important relaxation is expected. This redshift is maximum for 400-nm-wide QD's (about 4 meV), and then decreases in smaller structures. The redshift is weaker in QWR's, but also exhibits a maximum at about 400 nm. Moreover, in large structures, the shift is the same for both 25-Å and 165-Å-thick QW's. In the smallest QWR's and QD's structures a strong blueshift is observed.

These results are not in agreement with the theory, which predicts strong (up to 10 meV) and thickness-dependent blueshifts in the structures. Since the observed redshifts do not depend on the thickness of the QW in large structures, a mechanism involving the buffer rather than the QW's should be considered. As the lattice mismatch between the buffer and the substrate is rather high ($\epsilon_{\|}=-1.03\%$), the buffer may not be fully relaxed before etching.[37] There may remain some compressive in-plane stresses in the buffer, which will lessen the tensile strains in the overlying ZnTe QW's. After etching of the QWR's and QD's, these remaining strains relax even in wide structures since the aspect ratio of the etched buffer is very small (etching depth about 300 nm). As a consequence, the ZnTe QW's undergo higher tensile strains after etching than they did before. They thus exhibit an additional redshift, which is almost independent of their thickness, since this effect only involves the etched buffer. In small QWR's and QD's, the strain relaxation in the QW will bring back the PL peaks towards blue, as discussed before.

X-ray diffraction and preliminary cathodoluminescence experiments at 77 K support the assumption of local inhomogeneities in the buffer, which would relax with the etching process.

One can evaluate the strains in the buffer using the model developed in the former sections. The calculated shifts in the center of the structure are reported in Fig. 12(b) when a remaining in-plane strain $\epsilon=-0.14\%$ is imposed at the top of the buffer. After etching, there is a competition between the relaxation of the QW (which shifts the PL peaks towards blue) and the relaxation of the buffer (which shifts the PL peaks towards red). In the smallest structures, both the QW and the buffer have relaxed strains, but the relaxation of the QW is the dominant effect, resulting in small blueshifts. In structures of intermediate sizes (250–500 nm), the buffer has relaxed most of its strains but not the QW, resulting in a maximum redshift. Last, in large structures, the buffer cannot relax all strains any more, and the redshift decreases.

VI. CONCLUSION

In this paper we have discussed the inhomogeneous strain relaxation in etched QD's by making use of methods that have previously succeeded in describing etched QWR's. The complete calculation of strain relaxation was performed by using either continuum elasticity theory (finite elements method) or Keating's valence force field framework, which models the elastic properties on the atomic scale. For the investigated nanostructure sizes, the two methods appear to be equivalent. Several systems (II-VI/III-V, tensile/compressive, and a wide range of aspect ratio) have been considered. First we have shown that the relaxation ratio at the center of the stucture follows the same ''universal law'' for QWR's and QD's. From the strain distribution we have derived the piezoelectric potential and the band-edge variations in the nanostructures. The calculated band-gap energy in $CdTe/Cd_xZn_{1-x}Te$ systems is blueshifted, in reasonable agreement with experimental exciton energy shifts. However, a precise comparison would require a complete calculation of excitonic transitions, taking into account the strain-induced variations of the effective masses in the structure. Last, we have grown additional structures under tensile strains. For these structures, we have experimentally shown that the etching process has significant effects on the strain state of the buffer, which appears not to be fully relaxed.

ACKNOWLEDGMENTS

The authors thank C. Vieu (CNRS Bagneux) for the electron-beam lithography and the IBE etching and Professor G. Bauer, Dr. G. Brunthaler, and Dr. H. Straub for communicating unpublished results on the piezoelectric effect in quantum wires, and for stimulating discussions. Y.M.N. would like to thank GDR ''Matériaux pour l'optique non lineaire'' for financial support. This work has been partly supported by France Telecom (Contract No. 96 1B002). The ''Institut d'Electronique et de Microélectronique du Nord'' (IEMN) is ''Unité mixte 9929 du Center National de la Recherche Scientifique.''

*Present address: Institute for Micro- and Optoelectronics, Dept. of Physics, EPFL, CH-1015 Lausanne, France.

[1] M. Illing, G. Bacher, T. Kummell, A. Forchel, T. G. Andersson, D. Hommel, B. Jobst, and G. Landwehr, Appl. Phys. Lett. **67**, 124 (1995).

[2] G. Bacher, M. Illing, R. Spiegel, T. Kümmell, K. Herz, A. Frochel, B. Jobst, D. Hommel, and G. Landwehr, in Proceedings of the 7th Conference on II-VI Compounds, Edinburgh [J. Cryst. Growth **159**, 455 (1996)].

[3] P. Ils, M. Michel, A. Forchel, I. Gyuro, M. Klenk, and E. Zielinski, Appl. Phys. Lett. **64**, 496 (1994).

[4] A. Izrael, B. Sermage, J. Y. Marzin, A. Ougazzaden, R. Azoulay, J. Etrillard, V. Thierry-Mieg, and L. Henry, Appl. Phys. Lett. **56**, 830 (1990).

[5] W. Walecki, W. R. Patterson, A. V. Nurmikko, H. Luo, N. Sarmarth, J. K. Furdyna, M. Kobayashi, S. Durbin, and R. L. Gunshor, Appl. Phys. Lett. **57**, 2641 (1990).

[6] H. Straub, G. Brunthaler, W. Faschinger, G. Bauer, and C. Vieu, in Proceedings of the 7th Conference on II-VI Compounds, Edinburgh [J. Cryst. Growth **159**, 451 (1996)].

[7] L. De Caro and L. Tapfer, Phys. Rev. B **51**, 4381 (1995).
[8] C. Gourgon, H. Mariette, Le Si Dang, N. Pelekanos, C. Vieu, H. Straub, D. Stifter, and G. Brunthaler, *Proceedings of the Nanostructures Physics and Technology International Symposium, St. Petersburg, 1996* (Russian Academy of Sciences, St. Petersburg, 1996), p. 272.
[9] H. Straub, G. Brunthaler, W. Faschinger, G. Bauer, and C. Vieu, Proceedings of the XXIV International School of Physics of Semiconducting Compounds, Jaszowiec, 1996 [Acta Phys. Pol. A **90**, 1085 (1996)].
[10] G. Pickett, J. Appl. Mech. **A**, 176 (1944); S. P. Timoshenko and J. N. Goodier, *Theory of Elasticity* (McGraw-Hill, New York, 1970).
[11] M. J. P. Musgrave and J. A. Pople, Proc. R. Soc. London, Ser. A **268**, 464 (1962).
[12] M. Grundmann, O. Stier, and D. Bimberg, Phys. Rev. B **52**, 11 969 (1995).
[13] S. C. Jain, A. H. Harker, A. Atkinson, and K. Pinardi, J. Appl. Phys. **78**, 1630 (1995).
[14] D. A. Faux, J. Appl. Phys. **75**, 186 (1994).
[15] J. R. Downes and D. A. Faux, J. Phys.: Condens. Matter **9**, 4509 (1997).
[16] D. A. Faux, J. R. Downes, and E. P. O'Rielly, J. Appl. Phys. **80**, 2515 (1996).
[17] J. R. Downes, D. A. Faux, and E. P. O'Reilly, J. Appl. Phys. **81**, 6700 (1997).
[18] L. De Caro, L. Tapfer, and A. Giuffrida, Phys. Rev. B **54**, 10 575 (1996).
[19] Y. M. Niquet, C. Priester, and H. Mariette, Phys. Rev. B **55**, R7387 (1997).
[20] Y. M. Niquet, C. Gourgon, C. Priester, Le Si Dang, H. Mariette, C. Vieu, H. Straub, G. Brunthaler, A. Darhuber, T. Grill, W. Faschinger, in Proceedings of the 8th Conference on II-VI Compounds, Grenoble, 1997 [J. Cryst. Growth **184–185**, 334 (1998)].
[21] H. Straub, Ph.D. thesis, Universität Linz, 1997.
[22] P. N. Keating, Phys. Rev. **145**, 637 (1966).
[23] R. M. Martin, Phys. Rev. B **1**, 4005 (1970).
[24] J. L. Martins and A. Zunger, Phys. Rev. B **30**, 6217 (1984).
[25] I. H. Tan, R. Mirin, T. Yasuda, E. L. Hu, J. Bowers, C. B. Prater, P. K. Hansma, M. Y. He, and A. G. Evans, J. Vac. Sci. Technol. B **10**, 1971 (1992).
[26] Ch. Gréus, L. Butov, F. Daiminger, A. Forchel, P. A. Knipp, and T. L. Reinecke, Phys. Rev. B **47**, R7626 (1993).
[27] M. A. Haase, J. Qiu, J. M. Depuydt, and H. Cheng, Appl. Phys. Lett. **59**, 1272 (1991).
[28] *Physics of II-VI and I-VI Compounds, Semimagnetic Semiconductors*, edited by K.-H. Hellwege and O. Madelung, Landolt-Börnstein New Series, Group III, Vol. 17, Pt. b (Springer-Verlag, Berlin, 1982).
[29] J. M. Hartmann, J. Cibert, F. Kany, H. Mariette, M. Charleux, P. Alleysson, R. Langer, and G. Feuillet, J. Appl. Phys. **80**, 6257 (1996).
[30] M. Dauge, *Elliptic Boundary Value Problems on Corner Domains, Smoothness and Asymptotics of Solutions*, Lecture Notes in Mathematics Vol. 1341 (Springer-Verlag, Berlin, 1988).
[31] D. L. Smith and C. Mailhiot, Rev. Mod. Phys. **62**, 173 (1990).
[32] R. André, C. Deshayes, J. Cibert, Le Si Dang, S. Tatarenko, and K. Saminadayar, Phys. Rev. B **42**, 11 392 (1990).
[33] G. Bir and E. Pikus, Sov. Phys. Solid State **1**, 1502 (1960); See also G. Bir and E. Pikus, *Symmetry and Strain Induced Effects in Semiconductors* (Wiley, New York, 1974).
[34] Y. S. Tang, P. D. Wang, C. M. Sotomayor Torres, B. Lunn, and D. E. Ashenford, J. Appl. Phys. **77**, 6481 (1995).
[35] C. Gourgon, B. Eriksson, Le Si Dang, H. Mariette, and C. Vieu, Proceedings of the 6th Conference on II-VI Compounds, Newport [J. Cryst. Growth **138**, 590 (1994)]; Appl. Phys. Lett. **66**, 1635 (1995).
[36] H. Mariette, C. Gourgon, J. Cibert, Le Si Dang, C. Vieu, G. Brunthaler, H. Straub, W. Fashinger, N. Pelekanos, and W. W. Rühle, in *Semiconductor Heteroepitaxy* (World Scientific, Singapore, 1995), p. 383.
[37] E. A. Fizgerald, Mater. Sci. Rep. **7**, 87 (1991).